Influences on ionization fraction in an inductively coupled ionized physical vapor deposition device plasma

Daniel R. Juliano,[a] David N. Ruzic,[b] Monica M. C. Allain, and Douglas B. Hayden[a]
Department of Nuclear, Radiological, and Plasma Engineering, University of Illinois, 103 S. Goodwin Ave., Urbana, Illinois 61801

A computer simulation was created to model the transport of sputtered atoms through an ionized physical vapor deposition (IPVD) system. The simulation combines Monte Carlo and fluid methods to track the metal atoms that are emitted from the target, interact with the IPVD plasma, and are eventually deposited somewhere in the system. Ground-state neutral, excited, and ionized metal atoms are tracked. The simulation requires plasma conditions to be specified by the user. Langmuir probe measurements were used to determine these parameters in an experimental system in order to compare simulation results with experiment. The primary product of the simulation is a prediction of the ionization fraction of the sputtered atom flux at the substrate under various conditions. This quantity was experimentally measured and the results compared to the simulation. Experiment and simulation differ significantly. It is hypothesized that heating of the background gas due to the intense sputtered atom flux at the target is primarily responsible for this difference. Heating of the background gas is not accounted for in the simulation. Difficulties in accurately measuring plasma parameters, especially electron temperature, are also significant   © *2002 American Institute of Physics.* [DOI: 10.1063/1.1425447]

I. INTRODUCTION

Ionized physical vapor deposition (IPVD) for directional deposition of metal atoms has been widely investigated in recent years. The technique combines ionization of the incident sputter flux with a substrate potential lower than that of the local plasma.[1–6] The plasma sources used for ionization have included inductively coupled, electron–cyclotron resonance, helicon, and hollow cathode magnetron.

Since the purpose of these systems is to ionize the sputtered atoms incident on the substrate, the touchstone for these systems is the sputter flux ionization fraction; that is, the fraction of the sputtered atoms incident on the substrate that have been ionized by the secondary plasma.

Investigations into these systems has left many of the basic processes in these systems unexplained. Through the use of a combined Monte Carlo–fluid sputtered atom transport model, this work aims to rectify this situation. The relationship between the ionization fraction and various system parameters, such as plasma potential profile, electron temperature, plasma density, pressure, and background gas temperature are explored and explained for one type (inductively coupled) of IPVD system.

The hybrid Monte Carlo–fluid technique is used in this work in order to overcome limitations of either a purely Monte Carlo or purely fluid technique. The pressures of interest are low enough that a purely fluid model would not be accurate. Mean free paths for the higher energy sputtered atoms are a significant fraction of the chamber size: 43 mm

for a 100 eV copper atom in 35 mTorr of 300 K argon. But a direct Monte Carlo simulation[7] would be inefficient, because the lower-energy, thermalized sputtered atoms have small mean free paths: 5 mm for a 300 K copper atom in 35 mTorr of 300 K argon.[8] Therefore, a hybrid approach is used, in which the Monte Carlo technique is used to track high energy atoms (with long mean free path) and a fluid model is used to track low energy atoms (with small mean free path).

II. THE SYSTEM

The simulated system corresponds to an experimental ionized magnetron sputtering system detailed elsewhere,[8–11] shown schematically in Fig. 1.

The system was originally designed to handle 200 mm wafers. It has been modified by lowering the substrate holder and increasing the throw (target-to-substrate) distance from the original 83 mm to 155 mm. The chamber is 406 mm wide and holds a target 330 mm in diameter. The chamber bottlenecks to just 219 mm, however, just above the substrate holder. The substrate was originally at this level, making it flush with what was then the bottom of the chamber but which is now called the "shelf." Copper coils carrying rf current at 13.56 Mhz are placed inside the chamber, near the outside wall between the target and shelf. These coils power the secondary plasma that ionizes the sputtered atoms. While the system under study uses an inductively coupled plasma as the secondary source, the nature of the results should generalize to other types of plasma sources.

Typical operating pressures for IPVD are between 10 and 50 mTorr Ar. The sputter source for the system under study is a copper target powered by dc current, with a total power of 1 to 20 kW. The rf coils that are used to create the secondary plasma are typically driven by hundreds of watts.

[a]Present address: Novellus Systems, Inc., 4000 North First Street, San Jose, CA 95134

[b]Author to whom correspondence should be addressed; electronic mail: druzic@uiuc.edu
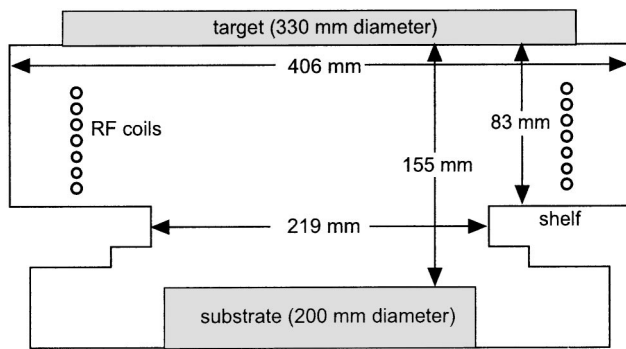
FIG. 1. Schematic of ionized magnetron sputtering system showing inductive coil.

III. THE MODEL

In the system under study, metal atoms travel from the target to the substrate through a vacuum chamber. At the pressures of interest to IPVD (10–50 mTorr), sputtered metal atoms have many collisions with the background gas and plasma on their journey to the substrate. In fact, most of the sputtered atoms end up back on the target or on the chamber walls (in excess of 80% for Cu in 35 mTorr Ar, for example). Of those that reach the substrate, a certain fraction have been ionized by the plasma, while the rest are neutral. This sputtered atom transport process has been modeled using a custom FORTRAN code called Sputtered Atom Transport in IPVD Systems (SATIS).

Sputtered atoms emerge from the target with a significant amount of energy (several to tens of eV), and are tracked individually via a Monte Carlo routine. The starting locations on the target are determined from experimental measurements of actual sputtered magnetron targets. The emitted atoms are launched with a cosine angular distribution,

$$P(\theta)d\Omega \propto \cos\theta d\Omega \tag{1}$$

$$\propto \cos\theta \sin\theta d\theta d\phi, \tag{2}$$

in which the probability of emission into a solid angle $d\Omega$ is proportional to the cosine of the angle to the normal θ. The energy of the emitted atoms is given by a Thompson distribution[12,13]

$$P(E)dE \propto \frac{E}{(E+E_b)^3}dE \tag{3}$$

where E_b is the binding energy of the sputtered material (3.5 eV for Cu). These simple distributions yielded results similar to those found using more detailed and accurate angular and energy emission distributions supplied by VFTRIM[14] calculations.

During each step in the Monte Carlo routine, the sputtered atom steps forward a random distance determined by its total collision cross section, which includes a variety of collision cross-sections including elastic collisions with background gas atoms, excitation and ionization collisions with plasma electrons, and several types of inelastic collisions with background gas atoms.

These collision cross-sections are compiled from a variety of sources. Cross sections for elastic collisions between sputtered atoms and background gas atoms are calculated using a combination Lennard–Jones and Ziegler-Biersack-Littmark (ZBL)[15] interatomic potential. Reaction rates for inelastic collisions with background gas atoms are borrowed from the Hybrid Plasma Equipment Model of Mark Kushner.[16] Cross-sections for inelastic collisions with electrons are calculated with a Boltzmann solver, which is a code designed to numerically solve the Boltzmann equation for the case where the only external force on the electrons is a uniform electric field:

$$\frac{\partial f}{\partial t} + \boldsymbol{v}\cdot\boldsymbol{\nabla}_r f + \frac{q\mathbf{E}}{m}\cdot\boldsymbol{\nabla}_v f = \frac{\partial f}{\partial t}\bigg|_c . \tag{4}$$

Here, $f(\mathbf{r},\boldsymbol{v},t)$ is the electron energy distribution. The term on the right side of the equation is the collision term, and includes all types of collisions. Solving this equation numerically for a given gas composition and given electric field yields an electron energy distribution f which can be roughly summarized by an electron temperature T_e, equal to 2/3 the average electron energy. The stronger the electric field $\mathbf{E}$, the higher the resultant electron temperature T_e. The reason the Boltzmann solver is useful is that the various collision rates are strongly dependent on the particulars of the electron energy distribution, which change depending on gas composition (even for the same average electron energy or temperature). The Boltzmann solver is used to calculate the proper collision rates for the particular gas compositions used in this simulation, at the various electron temperatures likely to be encountered during simulation.

At the site of a collision, the sputtered atom will change its velocity and may change electronic state depending on the collision type. It then steps forward to its next collision. After the sputtered atoms have lost most of their energy and are at the background gas temperature (are "thermalized"), their position is stored for later reference and another Monte Carlo flight run. Once all the Monte Carlo flights have run, all the previously stored atoms are entered into a bulk drift–diffusion routine that follows them until the vast majority of them have deposited on one of the surfaces in the simulation. During both the Monte Carlo and hybrid routines, atoms can react with the background plasma, changing electronic state. In this way the code can predict the flux of both neutral and ionized sputtered atoms on all surfaces.

The code assumes cylindrical symmetry and therefore uses cylindrical coordinates throughout. Because of this, SATIS can be considered to be a 2-dimensional simulation. The third, azimuthal, direction is tracked, but all results are averaged over that coordinate.

SATIS first loads the input information and processes it to set up various variables. The input file specifies primarily the system geometry, sputtered atom parameters, and background gas and plasma conditions. One of the most important input variables SATIS keeps track of is the gas composition in each mesh zone. The elements involved in the simulation each have several possible electronic states, each of which is tracked and referred to as a separate "species." The relative densities of the various atomic species are re-

ferred to as the "species fractions." It is difficult for a user to know what are reasonable initial values for these, so SATIS provides default values. Since the initial values could be quite different from the self-consistent values, SATIS iterates to converge to the proper species fractions. This information is therefore also one of the outputs of SATIS. When running several cases with small differences, the species fractions output from one case can be used as inputs to the next, reducing net simulation time.

For each cycle of the iteration procedure, SATIS launches a user-specified number of Monte Carlo flights from the target. Those flights that lose most of their energy have very small mean free paths and are considered thermalized. They then enter the fluid portion of SATIS, where they diffuse to the walls.

In both the Monte Carlo and diffusion routines, particles that hit the target are relaunched. This is a necessary consequence of starting atoms according to the net erosion of the target (rather than the gross emission distribution). This is an important step because at the pressures of interest, approximately 80% of the particles launched will return to the target, while only 20% will make it to the substrate or to a wall. Each relaunched particle must start in the Monte Carlo routine, so the diffusion routine is periodically halted while particles that have hit the target are relaunched via the Monte Carlo routine until they either hit a wall or re-enter the diffusion routine. The diffusion routine is then resumed.

Once most of the particles have hit walls, the results are collected and the species fractions updated. The cycle then starts over using the new values of the species fractions. Typically, about ten cycles are needed to converge these values. The number of cycles is specified by the user in the input file.

Further details on the workings of the code can be found in Ref. 8.

IV. RESULTS

Plasma potential, electron temperature, plasma density, and background gas temperature were varied and the resultant sputtered atom ionization fraction examined. By isolating the effects of each of these parameters, an understanding of their relative importance in the IPVD process can be gained.

The baseline case conditions were: background gas 35 mTorr Ar with temperature $T_{gas} = 400$ K everywhere, electron temperature $T_e = 2.0$ eV everywhere, electron density $n_e = 1 \times 10^{11}$ cm^{-3} everywhere, plasma potential $V_{plasma} = 30$ V with a 1 V presheath drop and 29 V drop in the sheath. In the subsections below, these are the parameters used unless otherwise specified.

A. Varying plasma potential

Neutral sputtered atoms are not affected by the plasma potential. However, ionized sputtered atoms feel an electric field produced by the gradient of the plasma potential. Once the sputtered atoms are thermalized, the neutral sputtered atoms diffuse, while the ionized sputtered atoms are both diffusing and drifting in the electric field. The importance of this electric field was examined by running four cases with different plasma potential profiles.
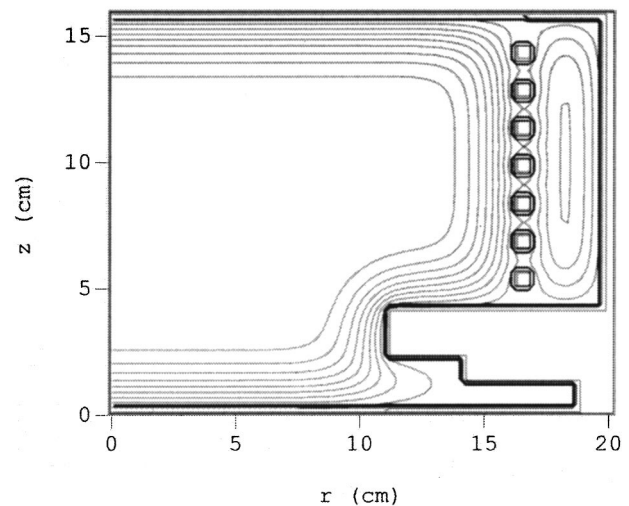

FIG. 2. Plasma potential in the simulated region. Contours are shown at 0.25 V intervals. Center of region is at 30 V; sheath edge is at 29 V.

The plasma potential used for most cases discussed in this work is shown in Fig. 2. This plasma potential profile is quite flat, with most of the 1 V presheath drop occurring near the edges. The 1 V presheath drop used was half the electron energy of 2 eV, as is typical of a dc sheath.[17]

This "flat" profile may be compared with that used in another case that was run, in which the plasma potential profile was much more rounded, dropping the 1 V of the presheath over a much wider region. This profile is shown in Fig. 3.

Another case was run with a flat shape identical to that shown in Fig. 2, but with a 10 V (instead of 1 V) presheath drop, meaning that the plasma potential contour plot is identical, but that the contours are at 1 V intervals. This variation is important because the assumption that the presheath drop is half of the electron temperature is derived for a dc sheath, whereas this is an rf plasma. This case will test if the results are sensitive to small differences in the presheath.
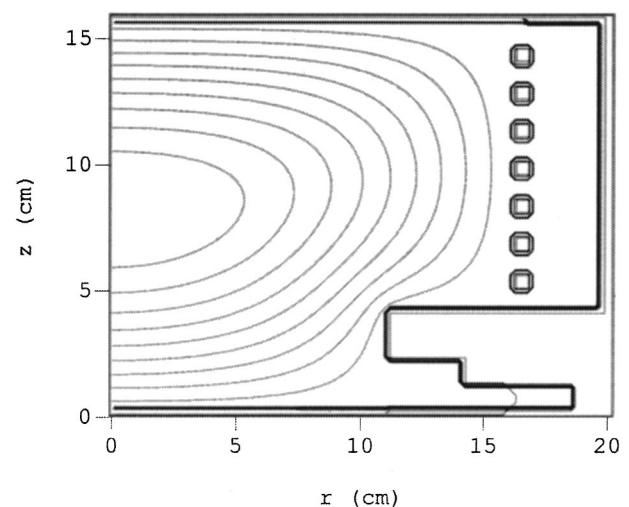

FIG. 3. Plasma potential in the simulated region for the "rounded" case. Contours are shown at 0.1 V intervals. Peak is 30 V, in center of region; sheath edge is at 29 V.
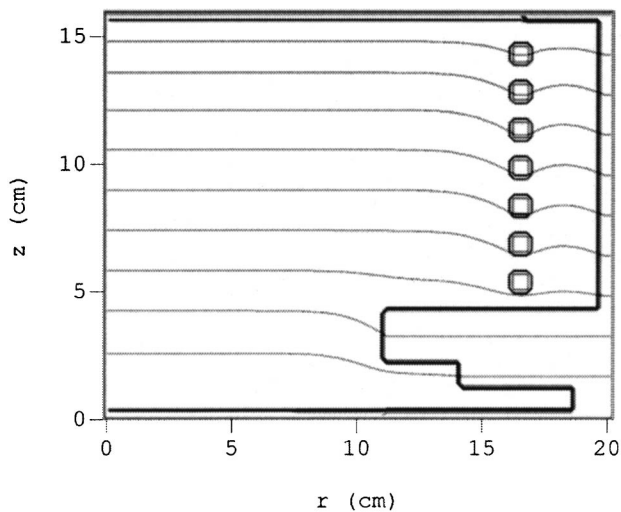
FIG. 4. Plasma potential in the simulated region for the "sloped" case. Contours are shown at 1.6 V intervals. Plasma potential near substrate is at 29 V; plasma potential near target is 13 V.
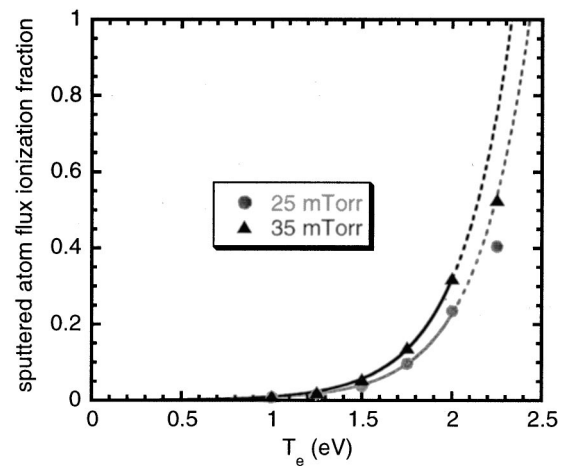

FIG. 5. SATIS flux ionization fraction as function of electron temperature with exponential curve fit to lowest five temperature points.

In fact, Langmuir probe measurements (detailed in Ref. 8) indicate that for the system under study, under many conditions the plasma potential is sloped across the system, with high voltage near the substrate and low voltage near the target. Therefore, a case was run in which the plasma potential slopes from 30 V near the substrate to 13 V near the target. This plasma potential profile is shown in Fig. 4.

The primary result of SATIS is the ionization fraction of the sputtered atom flux at the substrate. For all of these cases, this ionization fraction was virtually identical. The results are shown in Table I. In this table and throughout this work, the term "flux ionization fraction" refers to the fraction of sputtered metal atoms reaching the center of the substrate that are ionized.

In Table I, three significant figures are shown for the flux ionization fraction. Although the systematic uncertainty associated with these quantities is relatively large (perhaps 20% or more) the statistical uncertainty is less than ± 1 in the last digit shown. All three digits shown are needed in order to see the very slight change in ionization fraction as the plasma potential profile is changed.

B. Varying electron temperature

Four different cases were run in which the electron temperature was varied. In all cases, it was uniform across the system. Results are plotted in Fig. 5.

Electron temperature affects the ionization fraction directly through the rate of electron impact ionization, and in-

directly through an increase in the density of species such as Ar* and Ar$^+$, which can ionize the sputtered atoms through collisions. At low electron temperature, the ionization fraction rises approximately exponentially with electron temperature. This is reasonable because the population of high energy electrons rises exponentially with electron temperature, and these are the electrons that contribute to ionization of the sputtered atoms, both directly and indirectly as mentioned above. Specifically, the population of high energy electrons that increases exponentially with temperature is the population that has an energy several times the electron temperature. The population of interest for ionization of sputtered Cu atoms has an energy of at least 7.74 eV, which is the ionization potential of Cu. It is this population that increases exponentially with T_e.

In Fig. 5, although the ionization fraction increases exponentially with electron temperature for ionization fractions much less than 1, the ionization fraction cannot be higher than 1, and so cannot increase exponentially forever. By 2.25 eV, the ionization fraction has begun to saturate. Raising the electron temperature further would probably enter a regime in which the ionization fraction exponentially approached an asymptotic value of 1. The curve shown is an exponential fit to the points excluding the highest electron temperature (2.25 eV). It is clear in the figure that the fit is good at lower temperatures, but not above 2 eV. There is a distinct difference in ionization fraction for 25 mTorr compared to 35 mTorr. Both relationships are exponential, but the ionization fraction is higher at higher pressure. Given a constant ionization rate, the ionization fraction is directly proportional to the residence time of the sputtered atoms. Since the plasma used in the simulation at these two pressures was identical, the ionization rate is identical, and since the residence time is directly proportional to the pressure, the ionization fraction is also directly proportional to the pressure.

C. Varying plasma density

Five cases with different values for the plasma density were run. In all cases, the density was uniform across the system. Results are plotted in Fig. 6.

TABLE I. SATIS flux ionization fraction with different plasma potential profiles.

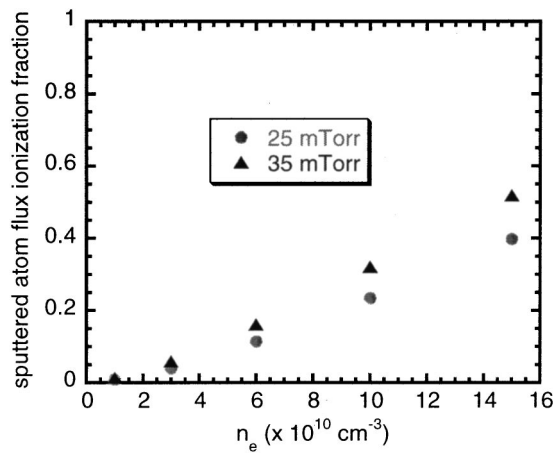| Plasma potential	Flux ionization fraction
Flat, 1 V presheath	0.321
Flat, 10 V presheath	0.324
Rounded, 1 V presheath	0.324
Sloped	0.324

FIG. 6. SATIS flux ionization fraction as function of plasma density.

Clearly, plasma density has a strong influence on the sputtered atom ionization fraction. Ionization due to electron impact is directly proportional to the electron density. And the species fractions of excited and ionized background atoms, which can ionize sputtered atoms through collisions, are also directly proportional to electron density. Therefore it is not surprising that the flux ionization fraction is nearly proportional to electron density. There is some deviation from this simple direct relationship because of the other processes involved, but the trend is clear. As with the electron temperature example, and for the same reasons, ionization fraction is directly proportional to pressure.

D. Varying background gas temperature

Four different cases were run in which the background gas temperature was varied. In all cases, it was uniform across the system. Results for the ionization fraction at the substrate and for total flux to the substrate are discussed in the sections that follow.

1. Effect on ionization fraction

The ionization fraction as a function of background gas temperature is plotted in Fig. 7. The temperature of the background gas is clearly very important for ionization of sputtered atoms. In fact, the ionization fraction is very nearly
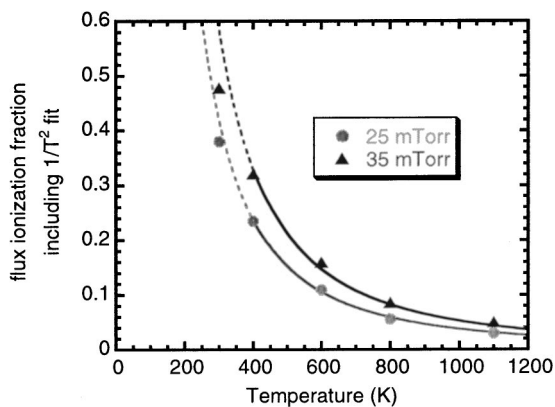

FIG. 7. SATIS flux ionization fraction as function of background gas temperature with inverse square curve fit to highest four temperature points.

inversely proportional to the square of the background gas temperature. There are very good reasons for this relationship.

As was discussed before, given a constant plasma (and therefore ionization rate) the ionization fraction (IF) is proportional to the residence time (τ_R) of the sputtered atoms:

$$IF \propto \tau_R \tag{5}$$

Therefore the relationship between background gas temperature and τ_R is important.

As the sputtered atoms diffuse they obey the diffusion equation:

$$\frac{\partial n}{\partial t} = -D\boldsymbol{\nabla}^2 n, \tag{6}$$

where

$$D = \frac{k_B T}{m v}, \tag{7}$$

with T the temperature of the sputtered atoms (equal to T_{gas}), m the mass of the sputtered atoms, and v the collision frequency. The larger the value of D, the faster the atoms diffuse and the shorter the τ_R:

$$IF \propto \tau_R \propto \frac{1}{D} \propto \frac{m v}{k_B T_{\text{gas}}}. \tag{8}$$

In this equation, m and k_B are constants. The collision frequency v is directly proportional to the background gas density n_{gas}, yielding

$$IF \propto \frac{n_{\text{gas}}}{T_{\text{gas}}}. \tag{9}$$

Since n_{gas} itself is inversely proportional to the background gas temperature, there is another factor of T in the denominator:

$$IF \propto \frac{1}{T_{\text{gas}}^2}. \tag{10}$$

These relations show that the ionization fraction is inversely proportional to the background gas temperature in two different ways, the net result being that the ionization fraction is inversely proportional to the square of background gas temperature. Again, there will be a saturation effect at high ionization fractions. This accounts for the slight deviation from the inverse square relationship seen in Fig. 7. The line on the plot is a fit to an inverse square relationship excluding the 300 K points, in which the ionization fraction has just begun to saturate, as is obvious by the fact that the points lie just below the curve fits.

2. Effect on total flux to the substrate

The variations discussed in previous sections do not affect the total sputtered atom flux to the substrate. The plasma potential, electron temperature, and electron density do not significantly affect the drifting and diffusion of the sputtered atoms; just the fraction of these atoms that become ions. However, the temperature of the background gas does affect the density of the background gas, which in turn affects the
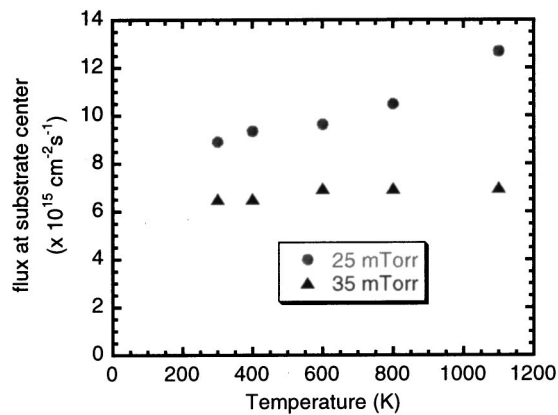
FIG. 8. SATIS total sputtered atom flux at the substrate center as function of background gas temperature.

chances that a sputtered atom will reach the substrate. At higher temperatures, the total sputtered atom flux to the substrate is slightly higher, as shown in Fig. 8.

In addition to the systematic uncertainty discussed earlier (which applies to all SATIS results) there is significant statistical uncertainty in the data plotted.

At first glance it might seem obvious that if the background gas is less dense, more atoms will reach the substrate than if it is more dense. The effect is more subtle than that, however.

There are three issues involved here. The diffusion of the sputtered atoms (neglecting drift, since it is of minor importance), nearly follows the inhomogeneous diffusion equation

$$\nabla^2 n(r,z) - \frac{1}{D}\frac{\partial n}{\partial t} = S(r,z), \tag{11}$$

where $S(r,z)$ is the diffusion source, the location of thermalization of the sputtered atoms, across the chamber. In steady state, which is the situation that is relevant here, this equation becomes simply

$$\nabla^2 n(r,z) = S(r,z). \tag{12}$$

The density distribution (and therefore the total sputtered atom flux to the substrate) only nearly follows this equation because the diffusion step size of the sputtered atoms is finite (about a quarter millimeter) rather than infinitesimal.

Another effect of changing the background gas temperature is that the diffusion constant D will change. For hotter (less dense) gas, D will increase. However, this will not affect the ultimate density distribution $n(r,z)$, because in the time-independent diffusion Eq. 12, which determines the density distribution $n(r,z)$, the diffusion constant D does not appear at all. The ultimate shape of the density profile is not affected by the magnitude of D.

The last way that changing the background gas temperature might affect the total flux to the substrate is through the source term $S(r,z)$. If the density of the background gas is lower, for instance, the high energy sputtered atoms will penetrate farther into the chamber before becoming thermalized. Therefore $S(r,z)$ will be farther from the target, closer to the center of the chamber. This will change the sputtered atom density distribution $n(r,z)$ and increase the total flux to the

substrate. The mechanism is not straightforward, so the relationship between background gas temperature and total flux at the substrate is not a simple one.

When the background gas temperature is changed by a certain factor, the mean free path of the sputtered atoms is changed by that same factor. At the lower pressure of 25 mTorr, the mean free path is larger than at the higher pressure of 35 mTorr. Therefore a change in the background gas temperature will have a larger effect on the mean free path at 25 mTorr than at 35 mTorr. The mean free path size governs the location of the diffusion source $S(r,z)$, therefore the variation of the background gas temperature will affect the diffusion source $S(r,z)$ more at 25 mTorr than at 35 mTorr. This is just what is seen in Fig. 8. At 25 mTorr, there is a definite positive correlation between background gas temperature and total flux to the substrate. At 35 mTorr the relationship is weaker, however.

V. EXPERIMENTAL VERIFICATION

Several SATIS cases were run using plasma conditions that were as realistic as possible, with plasma conditions that matched those measured in the real system using the Langmuir probe measurements. This was not always an easy task. The plasma potential, electron temperature, and plasma density profiles across the entire chamber had to be surmised from four points of measurement, each with substantial uncertainty. Some theoretical considerations were taken into account, but for the most part, the functions fit to the experimentally measured points are arbitrary, and were used simply because they seemed reasonable and fit the points well. The functions used to specify plasma parameters are summarized in Table II.

For the first case listed in Table II (35 mTorr, 2 kW sputter power), the experimentally measured sputtered atom flux ionization fraction was 0.075, and the fraction predicted by SATIS was 0.089. These number are quite close. This is encouraging, since the Langmuir probe data from this case was good, with multiple measurements yielding consistent results. The electron temperature was rather flat across the chamber in this case, making it easy to specify in SATIS.

For the second case listed in Table II (25 mTorr, 2 kW sputter power), the experimentally measured sputtered atom flux ionization fraction was 0.023, and the fraction predicted by SATIS was 0.161. This is quite a difference. It is possible the experimentally measured value was a bit low, but certainly not a factor of 7 too low. Also, lower pressures generally yield a lower ionization fraction, so the result would still be expected to be below the 35 mTorr value of 0.075, which is still less than half the value predicted by SATIS. The Langmuir probe data for this case was not especially good. In particular, the electron temperature was difficult to measure accurately and consistently. In fact, the same was true for the 700 W rf power case. The measurements have large uncertainties associated with them for these two 25 mTorr cases. This could easily explain the inflated value predicted by SATIS. If the electron temperature were, for example, 1.9 eV instead of 2.2 eV, this would reduce the ionization fraction by about 2/3, yielding a value of 0.054. This is a reasonable

TABLE II. Simulation conditions for realistic cases. It is assumed that values for r and z used in the equations are in cm. All cases used a background gas temperature of 400 K.

Pressure (mTorr)	Sputter power (kW)	rf power (kW)	Plasma potential (V)	T_e (eV)	n_e ($\times 10^{10}$ cm^{-3})
35	2	400	$30 - 2z$	2.0	$0.67 z J_0 \left(\dfrac{2.4r}{15} \right)$
25	2	400	$30 - z$	2.2	$0.67z$
35	1	400	$-50 + 25\sqrt{16-z}$	$1 + 0.33\sqrt{16-z} + 0.01r$	$2.5 + 0.09 z J_0 \left(\dfrac{2.4r}{25} \right)$
35	4	400	$25 - 0.8\sqrt{z^2 + r^2}$	$0.15 + 0.59\sqrt{z} + 0.01r$	$3.5 + 0.09 z J_0 \left(\dfrac{2.4r}{25} \right)$

value, though still somewhat higher than the experimentally measured value. But it is possible that the experimentally measured ionization fraction is too low. It is only 1/3 that measured at 35 mTorr. This seems a drastic reduction in the ionization fraction for a small pressure difference. In this case SATIS reveals the limitations of the experimental data. The measured ionization fraction and/or the Langmuir probe data (electron temperature in particular) are probably somewhat inaccurate.

For the third case listed in Table II (35 mTorr, 1 kW sputter power), the experimentally measured sputtered atom flux ionization fraction was 0.233, and the fraction predicted by SATIS was 0.056. The predicted ionization at this low power is too low by a factor of about 4.

Conversely, for the fourth case listed in Table II (35 mTorr, 4 kW sputter power), the experimentally measured sputtered atom flux ionization fraction was 0.022, and the fraction predicted by SATIS was 0.087. The predicted ionization at this high power is too high by a factor of about 4. While it is possible that the Langmuir probe data is not entirely accurate, it seems possibly more than coincidental that SATIS predicts an ionization that is too low at low sputter power and too high at high sputter power.

The one significant issue that is neglected by SATIS, which could account for the deviation from the experimentally measured values in these last two cases, is rarefaction of the background gas. It is known[18] that the high energy sputtered atoms coming from the target impart a significant amount of energy to the background gas in the target region. This stream of fast sputtered atoms coming from the target is sometimes called the "sputter wind." While the walls of the chamber will be near room temperature ($\sim$300 K) the background gas in the vicinity of the target might be much hotter.

This is apparent experimentally because when the sputter power is turned on, there is a jump in the chamber pressure before it stabilizes at its nominal value again. This indicates that the background gas is instantaneously heated by the sputter power. When the sputter power is turned off, the chamber pressure drops significantly before rising again to its nominal value. Because of this, the background gas temperature used for these realistic cases was 400 K, which is 100 degrees hotter than the chamber walls, which are at approximately 300 K. However, using a uniform warm temperature does not really fit reality. In reality, the gas near the target will be warmer while the gas far away will be cooler. In general, neglecting this effect should lead to the prediction of ionization fractions that are too high at high sputter powers. Gas rarefaction lowers the background gas density, lowering residence time and therefore the ionization fraction. It also allows the sputtered atoms to get closer to the substrate, passing through a rarefied region, before becoming thermalized. This means that more sputtered atoms will reach the substrate and fewer will reach the target. The higher the sputter power, the more important this effect will be. It was shown earlier that the ionization fraction varies inversely with the square of background gas temperature, so the coupling between rarefaction and ionization fraction is bound to be strong.

At the relatively low sputter power of 1 kW, it is possible that the rarefaction effect is minor, possibly so minor that using a 400 K background gas temperature is not justified. If the background gas temperature were really 300 K, this would nearly double the ionization fraction according to the simple cases discussed earlier. This would make the SATIS-predicted value much closer to the experimentally observed value. Conversely, at 4 kW sputter power, the rarefaction effect is surely significant. This effect could easily explain why the predicted value is higher than the measured value.

VI. CONCLUSION

SATIS simulations in which the plasma parameters were varied one at a time were instructive in elucidating the salient factors in ionized physical vapor deposition.

Because the electric fields involved are weak, the plasma potential profile is not important to the ionization fraction. The transport of ions is dominated by diffusion. This means, for example, that biasing the substrate negatively in order to slope the plasma potential toward it will not significantly increase the ionization fraction at the substrate. The flux ionization fraction was found to be exponential with electron temperature at low temperatures and ionization fractions, meaning that a small difference in electron temperature can cause a big difference in the ionization fraction. The ionization fraction is roughly proportional to plasma density and to background gas density (and therefore to pressure given a

constant background gas temperature), and varies inversely with the square of the background gas temperature. This is relevant to the background gas rarefaction that can occur due to intense sputter flux. All of these influences saturate at high ionization fractions, and the stated relationships no longer hold.

These relations can be summarized by the commonsense statement that the flux ionization fraction is proportional to the ionization rate and to the residence time within the ionizing plasma. Factors that influence either of these two properties will influence the flux ionization fraction. This holds true until the flux ionization fraction is high enough that it begins to saturate, and is no longer directly proportional to ionization rate and residence time.

The total sputtered atom flux to the substrate was independent of plasma potential, electron temperature, and electron density, but weakly dependent on background gas temperature. Hotter background gas is less dense, allowing the high energy sputtered atoms to penetrate farther into the chamber before becoming thermalized, after which their motion is diffusive. The change in this diffusion source term then results in a higher sputtered atom flux at the substrate.

ACKNOWLEDGMENTS

[1] W. Holber, J. S. Logan, H. J. Grabarz, J. T. C. Yeh, J. B. O. Caughman, A. Sugarman, and F. E. Turene, J. Vac. Sci. Technol. A **11**, 2903 (1993).
[2] M. Yamashita, J. Vac. Sci. Technol. A **7**, 151 (1989).
[3] S. M. Rossnagel and J. Hopwood, J. Vac. Sci. Technol. B **12**, 449 (1994).
[4] S. M. Rossnagel, Appl. Phys. Lett. **63**, 3285 (1993).
[5] P. F. Cheng, S. M. Rossnagel, and D. N. Ruzic, J. Vac. Sci. Technol. B **13**, 203 (1995).
[6] S. M. Rossnagel, J. Vac. Sci. Technol. A **16**, 2585 (1998).
[7] G. A. Bird, *Molecular Gas Dynamics and the Direct Simulation of Gas Flows* (Wiley, New York, 1964).
[8] D. R. Juliano, Ph.D. thesis, University of Illinois-Urbana, 2000.
[9] K. M. Green, D. B. Hayden, D. R. Juliano, and D. N. Ruzic, Rev. Sci. Instrum. **68**, 4555 (1997).
[10] D. B. Hayden, D. R. Juliano, K. M. Green, D. N. Ruzic, C. A. Weiss, K. A. Ashtiani, and T. J. Licata, J. Vac. Sci. Technol. A **16**, 624 (1998).
[11] D. B. Hayden, Ph.D. thesis, University of Illinois-Urbana, 1999.
[12] P. Sigmund, Phys. Rev. **184**, 383 (1969).
[13] M. W. Thompson, Philos. Mag. **18**, 337 (1968).
[14] M. A. Shaheen and D. N. Ruzic, J. Vac. Sci. Technol. A **11**, 3085 (1993).
[15] J. F. Ziegler, J. P. Biersack, and U. Littmark, in *Stopping and Ranges of Ions in Matter* (Pergamon, New York, 1985), Vol. 1, pp. 24–48.
[16] M. J. Grapperhaus, Z. Krivokapic, and M. J. Kushner, J. Appl. Phys. **83**, 35 (1998).
[17] M. A. Lieberman and A. J. Lichtenberg, *Principles of Plasma Discharge and Materials Processing* (Wiley, New York, 1994).
[18] M. Dickson, F. Qian, and J. Hopwood, J. Vac. Sci. Technol. A **15**, 340 (1997).